Experimental and numerical investigation of arching effect in sand using modified Mohr Coulomb

Golam Moradi [a] and Alireza Abbasnejad [*]

Department of Geotechnical Engineering, University of Tabriz, 29 Bahman Boulevard, Tabriz, Iran

Abstract. In the current paper the results of a numerical simulation that were verified by a well instrumented experimental procedure for studying the arching effect over a trapdoor in sand is presented. To simulate this phenomenon with continuum mechanics, the experimental procedure is modeled in ABAQUS code using stress dependent hardening in elastic state and plastic strain dependent frictional hardening-softening with Mohr Coulomb failure criterion applying user sub-routine. The apparatus comprises rectangular trapdoors with different width that can yield downward while stresses and deformations are recorded simultaneously. As the trapdoor starts to yield, the whole soil mass deforms elastically. However, after an immediate specified displacement, depending on the width of the trapdoor, the soil mass behaves plastically. This behavior of sand occurs due to the flow phenomenon and continues until the stress on trapdoor is minimized. Then the failure process develops in sand and the measured stress on the trapdoor shows an ascending trend. This indicates gradual separation of the yielding mass from the whole soil body. Finally, the flow process leads to establish a stable vault of sand called arching mechanism or progressive collapse of the soil body.

1. Introduction

The arching phenomenon is known to engineers as the reduction of stress experienced due to yielding part underground structure. Arching plays an important role in structure-soil interaction such as: excavation, retaining structures, pile group effects, tunnel boring machines, culverts and various underground facilities. When part of a soil mass yields, while other parts adjoining the yielding part remain stationary, movement between yielding and stationary parts causes shear stress to develop. This shear stress opposes the relative movement of soil masses. Since the shearing resistance tends to keep the yielding mass in its initial position, it reduces the pressure on the yielding part and increases it on the adjoining stationary. The essential features of arching were demonstrated by experiments on sand with a yielding trapdoor performed by Terzaghi. The shear plane theory was subsequently proposed by him in 1943. The analysis involved studying the

---

∗Corresponding author, Ph.D. Candidate, E-mail: abbasnejad_ar@yahoo.com
[a] Ph.D., E-mail: moradi_gholam@tabrizu.ac.ir

equilibrium horizontal element of soil, assuming that soil has perfectly plastic behavior (Terzaghi 1943). Later, experimental modeling the soil arching as the transfer of soil pressure from a yielding support to an adjacent non-yielding support, was done by several researches such as Vardoulakis *et al*. (1981), Otani and Chevalier (2010), Sadrekarimi and Abbasnejad (2010).

Experiments of Pardo and Sáez (2014) were based on Terzaghi's trapdoor test. The displacement field of the soil is estimated using the Digital Image Correlation (DIC) technique. In their numerical study two elasto-plastic constitutive models of increasing complexity were compared and examined for their ability to reproduce this phenomenon. Kim *et al*. (2013) studied the lateral earth pressure of vertical circular shaft. They introduced a framework for determining the earth pressure distribution on the basis of both centrifuge model and full-scale field test results. They found that the lateral earth pressure acting on a vertical circular shaft considering arching effect is 80% smaller than that calculated by Rankine theory. Hosseinian and Cheraghi Seifabad (2013) investigated arching effect of retained structure with anchorage method, Plaxis 3D Tunnel software was used to model fine-grain (CL-ML) with hardening soil behavior which simulates soil material. A comparison between the results gained from the 3D FE analyses and the more or less conventional method shows that the classical method is much more on the safe side. Dalvi and Pise (2012) investigated arching action considering passive earth pressure in non-cohesive backfill. The backfill was assumed to move upward in a form of catenary arch due to arching. An illustrative example was solved to show the effect of the angle of major principal plane on earth pressure distribution on retaining wall considering arching for different wall friction angles and soil friction angles and applicability of proposed formulation is compared with model test results.

Recently, the discrete element method (2D/3D DEM) has been employed to model the tunnel face failure considering arching effect (e.g., Chen *et al*. 2011). The coupled DEM/FEM method has also been used to investigate the earth pressure acting on the tunnel lining (the surrounding soil being modeled using DEM with the lining modeled using FEM (Dang and Meguid 2011). Sadrekarimi and Abbasnejad (2008, 2010) used an instrumented apparatus that comprises concentric circular trapdoors with different diameters that can yield downward while stresses and deformations are recorded simultaneously. They also compared the result with Terzaghi's theory and upper boundary solution suggested by Atkinson and Potts (1977). They also introduced an equation for the stable arch obtained from the experiment.

Modeling arching phenomenon in continuum mechanics and finding a soil model that can describe the behavior of the soil during arching especially in granular soils is the place of discussion. In spite of vast investigations on soil arching, there has not been an ample study done on the modeling of the arching effect considering the hardening and softening phenomenon occurred during it. Current paper presents results of a numerical and experimental work in which the best proper constitutive soil model is investigated.

2. Soil properties

The test soil was a cohesionless silty sand with passed percentage of 100% and 9% from sieves No. 10 and No. 200, respectively. The gradation curve coefficient of curvature C_c and coefficient of uniformity C_u were 1.1 and 5.3. The sieve test result is illustrated in Fig. 2. The soil was classified as SP-SM according to USCS and the maximum and minimum dry densities were measured as 17.01 and 12.63 kN/m3, respectively. The specific gravity of solid particles was 2.62 and the moisture content was kept at 2% throughout the experiments.
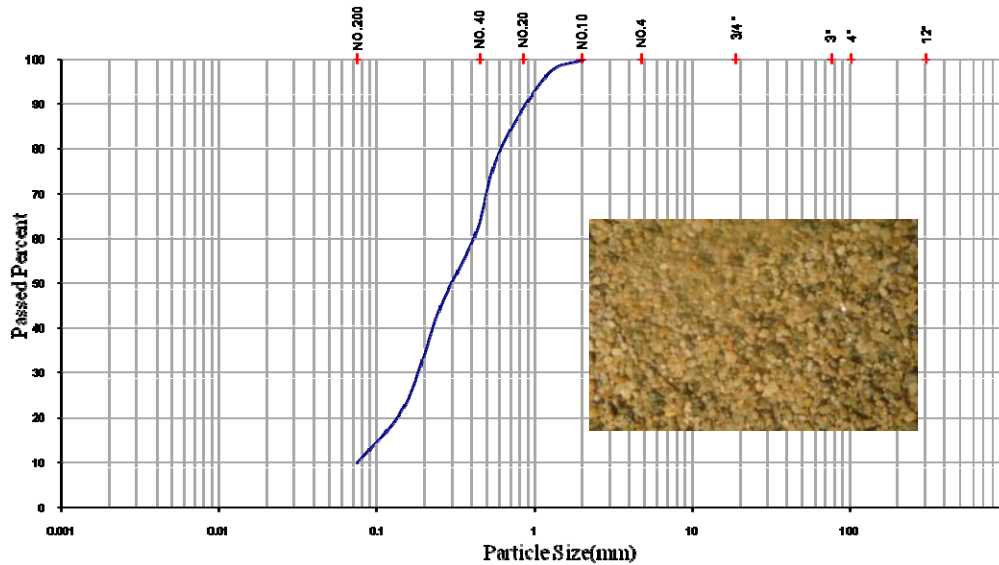
Fig. 1 Sieve analysis of the test soil

3. Finite-element modeling methodology

Numerical Modeling of the arching effect has been performed using "ABAQUS 2012" program with modifications in stress and strain hardening-softening model. Bray *et al*. (1994) concluded that FE modeling can be successful if certain conditions are satisfied, such as the use of a refined mesh in the neighborhood of the potential rupture with large deformations and the use of a nonlinear constitutive law for the soil.

ABAQUS provides a wide range of tools like Explicit Finite-Element-Method to solve geotechnical boundary value problems with moderate to large deformations. Also it uses couple Eulerian – Lagrangian (ALE) to solve large deformation boundary value problems that are limited to single phase analysis (ABAQUS User's manual 2012).

For simulating the arching effect a 2D model with plain strain assumption is performed. Model correction in this study is done via a subroutine written in FORTRAN code and linked to ABAQUS to define the plastic strain hardening and softening behavior and also dependency of elastic modulus to the mean stress.

4. Constitutive model

Several experimental and numerical studies have shown that post-peak soil behavior is a decisive factor in rupture propagation and its possible on the ground surface. Also pre-peak behavior has a significant rule on the stress hardening and strain hardening of the soil (Cole and Lade 1984, Vermeer and de Borst 1984). The hardening and softening behavior of soil using different soil models were also studied in different structures such as dams, soil nails and faults (Mahin Roosta and Alizade 2012, Ardakani *et al*. 2014, Anastasopoulos *et al*. 2007).

In this research we adopted Modified Mohr-Coulomb constitutive model with stress dependent

stiffness during elastic strains and strain hardening-softening dependency in plastic section both in pre and post peak zones.

4.1 Stress dependent elastic modulus

Pre-yield behavior is modeled as linear elastic with a secant shear modulus (G_S)

$$Gs = \frac{\tau_y}{\gamma_y} \tag{1}$$

where τ_y and γ_y are yield shear strain and stress, respectively. While γ_y can be directly measured from the test data (the shear stress that corresponds to $\delta\chi_y$). To compute γ_y, a shear zone thickness needs to be assumed. Before formation of the shear band, shear strain can be assumed to be more or less uniformly distributed throughout the whole depth, D, of the soil specimen. Hence, γ_y can be defined as

$$\gamma_y = \frac{\delta\chi_y}{D} \tag{2}$$

The same can be applied for the peak shear strain γ_p (assuming that the shear band has not yet formed)

$$\gamma_p = \frac{\delta\chi_p}{D} \tag{3}$$

Consequently, the plastic shear strain at peak will be

$$\gamma_p^p = \frac{\delta\chi_p - \delta\chi_y}{D} \tag{4}$$

The Young's modulus, E, was obtained from

$$E = \frac{9KG_s}{3K + G_s} \tag{5}$$

Where K is Bulk modulus. Both the bulk modulus, K, and the second shear modulus, Gs, are stress dependent and in order to take this dependency into account, the model uses the following equations

$$K = K_0 \left(\frac{P}{P_{ref}} \right)^b \tag{6}$$

$$G_s = G_0 \left(\frac{P}{P_{ref}} \right)^b \tag{7}$$

Where p_{ref} is the reference pressure for which $K = K_0$ and $G_s = G_0$. The pressure exponent, b, is a model parameter expressing the variation of the elastic modules with the isotropic pressure. The

value of b is reported to vary from 0.435, at very small strains, to 0.765, at very large strains according to Wroth (1979). A value of 0.5 captures most of the important features of increased shear stiffness with pressure (Wroth and Houlsby 1985).

Poisson's ratio (v) can be defined using the following equation

$$v = \frac{3K - 2G_s}{2(3K + G_s)} \tag{8}$$

In this research due to changes in stress state during the analysis, the elastic modulus is defined according to the normal stress.

4.2 Failure criteria and potential functions

In this research the soil model used for sand is an elasto-plastic constitutive model with Mohr-Coulomb failure criteria and isotropic strain hardening and softening which was adopted and encoded in the ABAQUS (2012) finite element environment. The Modified Mohr-Coulomb plasticity model is particularly useful to model frictional materials like sand or concrete. However, many enhancements have provided that it is suitable for all kinds of soil.

4.3 Frictional hardening

Vermeer and de Borst (1984) proposed Eq. (9) for frictional hardening behavior of geotechnical material, in which mobilized friction angle (φ_m) depends on plastic strain (γ_p) and gradually increases to reach the peak friction angle

$$\sin \varphi_m = 2 \left(\frac{\sqrt{\gamma_p \times \gamma_p^p}}{\gamma_p + \gamma_p^p} \right) \sin \varphi_p \tag{9}$$

Where, γ_p^p is shear plastic strain at peak friction angle φ_p.

The equation to present the variable dilation angle put forward by Rowe (1963) is called stress dilatancy equation and is as follows

$$\sin \Psi_m = \frac{\sin \varphi_m - \sin \varphi_{cr}}{1 - \sin \varphi_m \sin \varphi_{cr}} \tag{10}$$

$$\sin \varphi_{cr} = \frac{\sin \varphi_p - \sin \Psi_p}{1 - \sin \varphi_p \sin \Psi_p} \tag{11}$$

Where Ψ_m and φ_m are mobilized dilation angle and peak dilation angle, respectively. φ_{cr} is the critical friction angle or friction angle of constant volume. The mobilized dilatation angle is initially negative and increases with increase of plastic strain. To prevent this high value of negative dilation angle in small strains, following equation was presented by Soreide *et al.* (2002), which also is used in this paper in modeling dilation behavior of sand

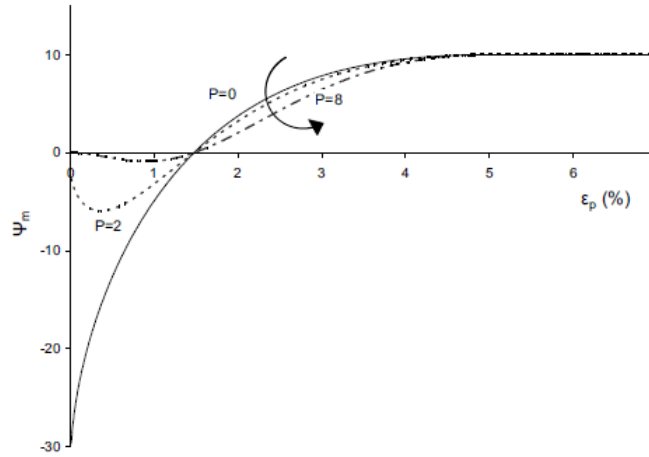$$\sin \Psi_m = \sin \Psi_p \left(\frac{\sin \varphi_m}{\sin \varphi_{cr}} \right)^p \tag{12}$$

Fig. 2 Variation of mobilized dilation angle with variation of *P*

Where, *P* is constant value and controls the shape of the curve. Variation of mobilized dilation angle with plastic strain is indicated in Fig. 2, for different values of power *P*. In the current paper the changes of mobilized dilation angle is assumed to have a linear relation with mobilized friction angle and *P* value is considered to be 1.

4.4 Frictional softenings

After formation of the shear band (i.e., right after the peak), adopting the two-block model of shearing of Shibuya *et al.* (1997), it is assumed that all plastic shear deformation takes place within the shear band, while the rest of the soil body remains elastic. Assuming the width of the shear band, d_B, equal to $16d_{50}$ (Vardoulakis and Graf 1985), where d_{50}, mean particle size of the sand, the plastic shear strain at which softening is completed, γ_f^p, will be

$$\gamma_s^p = \gamma_p^p + \frac{\delta\chi_p^p - \delta\chi_y}{16d_{50}} = \frac{\delta\chi_p^p - \delta\chi_y}{D} + \frac{\delta\chi_p^p - \delta\chi_y}{16d_{50}} \tag{13}$$

Strain softening is introduced by reducing the mobilized friction angle φ_m and the mobilized dilation angle Ψ_m with the increase of plastic octahedral shear strain

$$\varphi_m = \begin{bmatrix} \varphi_p - \dfrac{\varphi_p - \varphi_{res}}{\gamma_s^p}\gamma_{oct}^p & \text{for} & \gamma_p^p \leq \gamma_{oct}^p < \gamma_f^p \\ \varphi_{res} & \text{for} & \gamma_{oct}^p > \gamma_f^p \end{bmatrix} \tag{14}$$

$$\Psi_m = \begin{bmatrix} \Psi_p\left(1 - \dfrac{\gamma_{oct}^p}{\gamma_s^p}\right) & \text{for} & \gamma_p^p \leq \gamma_{oct}^p < \gamma_f^p \\ \Psi_{res} & \text{for} & \gamma_{oct}^p > \gamma_f^p \end{bmatrix} \tag{15}$$

where φ_p and φ_{cr} are peak mobilized friction angle and critical friction angle, respectively; Ψ_p is

peak dilation angle; and γ_s^p is plastic octahedral shear strain at the end of softening.

4.5 Meshing and other details

The use of the finite-element method in combination with strain softening constitutive models may lead to mesh-dependent solutions (e.g., Pietruszezak and Mroz 1981). To obtain mesh-independent solutions, the size of the elements has to be approximately $3d_{50}$ (Gudehus and Nübel 2004). Obviously, such mesh size prohibits the application of such rigorous approaches in modeling real-scale problems. To do so, remeshing for localization zones would be necessary (Gudehus and Nübel 2004). Scale effects have proven to be substantial in shear localization problems (Muir Wood and Stone 1994, Muir Wood 2002) and have to be carefully addressed. It must be clearly pointed out that shear localization can take place along one element, i.e., the width of FE shear "band" will be equal to the size of the element, d_{FE}, for four-node elements (or to half of it, for eight-node elements). So, ideally, d_{FE} should be equal to the width of the real shear band d_B ($16d_{50}$) (Anastasopoulos *et al*. 2007). In this research the limitation of the element size has been taken into account, too.

In the numerical models of this research the trapdoor is positioned under the soil model and connected to it through special contact elements, which are rigid in compression but tensionless, allowing detachment of the trapdoor from the soil, while positive normal force is transmitted. Both detachment and rigidity are important characteristics for realistic trapdoor modeling. For modeling the flow during arching phenomenon, the mesh size plays an important role, so the meshes around the trapdoor and also the parts that are predicted to have large deformations, are adopted with small mesh size. To eliminate the effect of dynamic analysis of explicit-dynamic analysis, the time defined to analyze is considered a large period so that the ratio of kinetic energy to internal energy would be less than 1 percent.

4.6 Stress dependent friction and dilation angle

Due to this fact that friction and dilation angles depend upon confining pressure, which also was observed in the laboratory tests, and in order to determine shear strength parameters corresponding to the relevant stress levels, direct shear tests under various surcharges were carried out. The magnitude of the internal friction angle φ depends on the magnitude of the state of the stress for a particular soil (Atkinson and Potts 1977). The lower the normal load the higher the φ angle. But according to the stress-dilatancy theory the void ratio, water content and dilatancy are also important as well as shear and normal effective stresses in analyzing the results and soil behavior. The stress- dilatancy criteria equation is given by

$$\frac{\tau}{\sigma} = \tan(\varphi_{cr} + \Psi) \tag{16}$$

In the above equation the angle of dilation Ψ depends on the initial state. So we modified the magnitude of the test results according to the stress-dilatancy theory. Shibuya *et al*. (1997) have shown that the simple shear mode only needs to be developed along the shear band. The relationship between the direct shear peak φ_p and residual or critical state angle of friction φ_{cr} can be approximated as

$$\tan\varphi_p = \tan\varphi_{cr} + \alpha \tan\psi_p \tag{17}$$

Where α is a constant value. With an optimum shear box apparatus (no rotation of the loading platen, smooth end walls, opening size between top and bottom platen equal to the thickness of the shear band) α can be taken equal to 1 (Shibuya *et al*. 1997). The plane strain peak angle of friction φ_p can then be computed as (Jewell 1989)

$$\sin \varphi_p = \frac{\tan \varphi_p}{\sin \Psi_p + \sin \Psi_p \tan \varphi_p} \tag{18}$$

Following the above researches, 21 simple direct shear tests are carried out on the mentioned sand. In these tests, parameters for sand in 3 different relative densities and 7 different applied normal pressures which was changed from 7 kPa to 300 kPa were studied. The results are illustrated in Figs. 3 and 4. The peak internal friction angle is modified using Eq. (17).
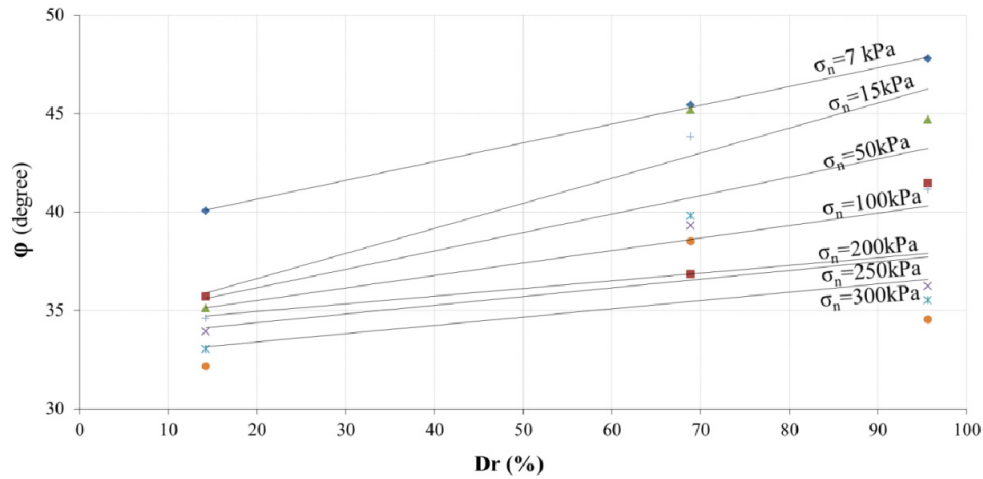

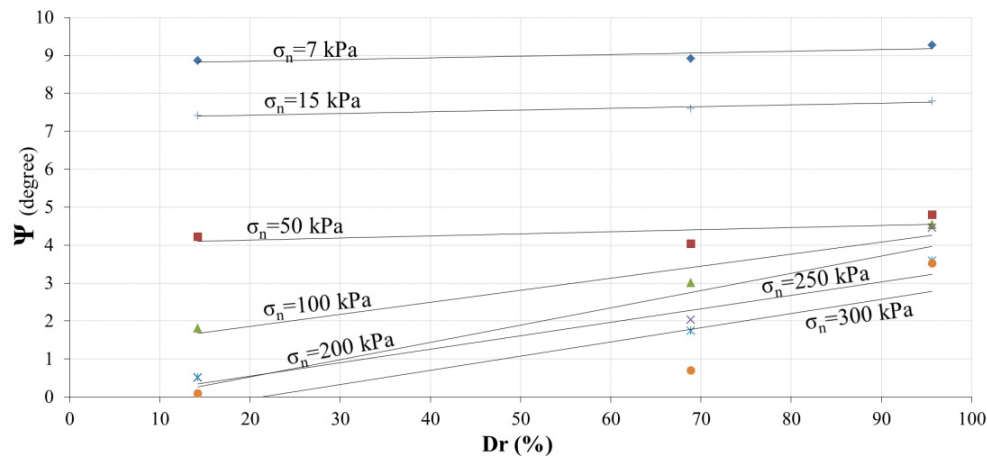Fig. 3 Internal friction angle φ against relative density

Fig. 4 Dilation angle Ψ against relative density

(a) Dense sand ($D_r = 95\%$)   (b) Loose sand ($D_r = 15\%$)
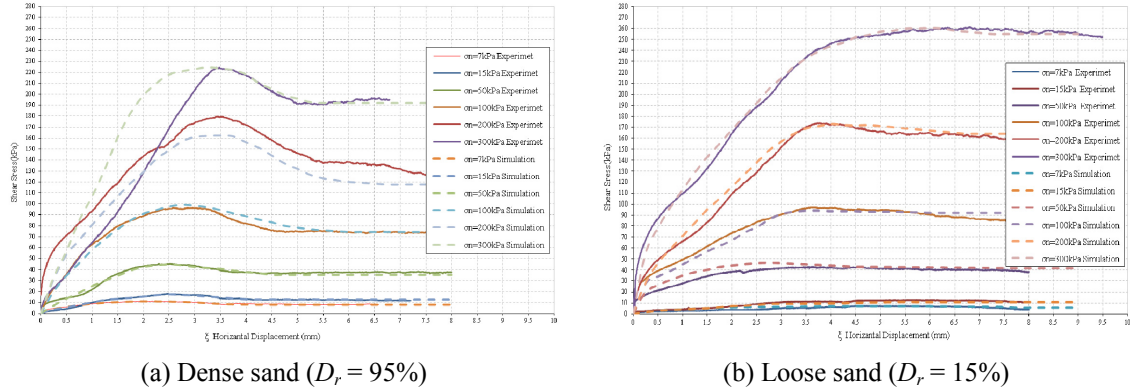
Fig. 5 Comparison between laboratory direct shear tests and the results of the constitutive model for dense sand

4.7 Constitutive model verification

To verify the capability of the modified Mohr-Coulomb constitutive model to reproduce actual soil behavior, a series of FE simulations of the direct shear test have been compared to laboratory data. Fig. 5 illustrates an example of model calibration for Loose and dense Sand ($d_{50} = 0.3$ mm) based on direct shear test. The initial depth of the soil sample was $D = 20$ mm and the vertical effective stress varied from 7 to 300 kPa.

As illustrated in Fig. 5, the comparison between simulated and laboratory curves are quite satisfactory. In conclusion, despite its simplicity and (perhaps) lack of generality, the constitutive model can capture adequately the predominant mode of deformation of the specific problem studied herein — a reasonable simplification to a complex soil behavior.

5. Experimental modeling

5.1 The model properties

An apparatus was designed and constructed. The whole system is schematically shown in Fig. 6. The sand container was 0.966 m³ in volume and 1.25 cm in height with a rectangular horizontal cross section with 0.4 m in width and 1.83 m in length. The container was made of 10 mm thick steel plate and 30 mm thick plaxy glass in both sides to observe the soil that strengthened with stiffeners. A general view of the apparatus is shown in Fig. 7. Three rectangular trapdoors with 10, 20 and 30 cm in width were constructed that can be installed under the base of the container, as shown in Figs. 6 and 8. The trapdoors are installed separately moving the adjoining plates sideward. The trapdoor yields downward by a hydraulic jack installed bellow. The load magnitudes on the trapdoors, caused by the pressure of the overburden soil, were measured using a load cell. The displacement of the trapdoors was monitored using Linear Variable Deferential Transformer (LVDT) installed under the platform and over the soil surface as shown in Fig. 8.

5.2 Test procedure

At the beginning, without any displacement, the normal stress $\sigma_\circ$ applied to the trapdoor is γh,
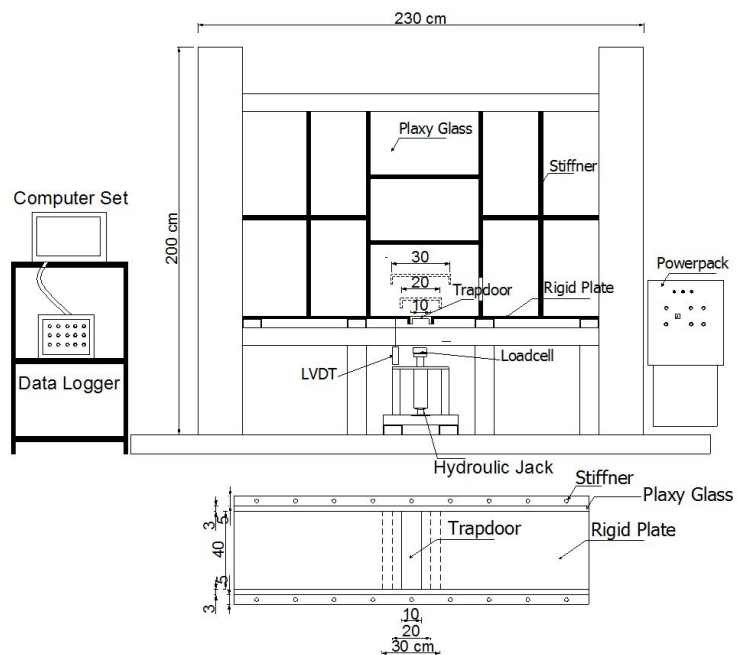
Fig. 6 Schematic diagrams of the apparatus
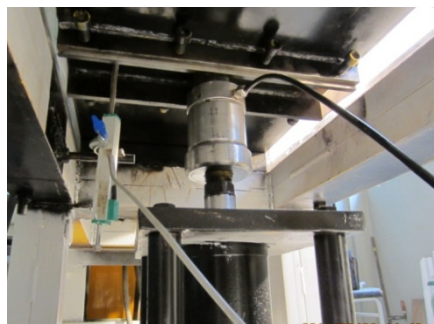

Fig. 7 General view of the test system

Fig. 8 Detail of the trapdoors, load cell and displacement gauge

in which *γ* is the density of the sand and h is the height of the mass of the sand in the container. In order to deposit the sand in loose condition it was poured from a defined height using a sand-rain system; and in order to produce dense sand each layer of sand was compacted evenly with compactor. Each layer of soil was 15 cm thick, and the time of the compacting was varied depending on the expected densities. This stage was very time consuming and several tests were carried out to make sure that the soil density was the same throughout the whole mass.

Having filled the container with sand, the nuts and bolts holding the trapdoor were unscrewed while the upward pressure on the trapdoor was being adjusted so that the trapdoor did not displace. This was a curtail point of course. At this stage the recorded stress was very close to *γh*. Following this stage the trapdoor was slowly yielded downward by hydraulic jack placed under the load cell. This trend continued until the load displayed by the load cell tended towards an asymptote.
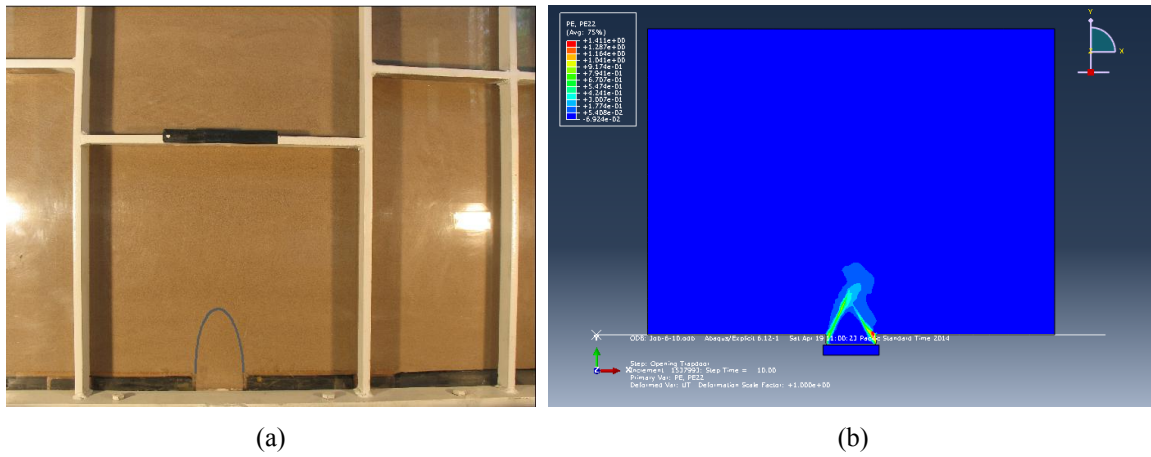

(a)   (b)

Fig. 9 Comparing the experimental formation of arching and plastic contours for 10 cm trapdoor diameter ($D_r = 14\%$)

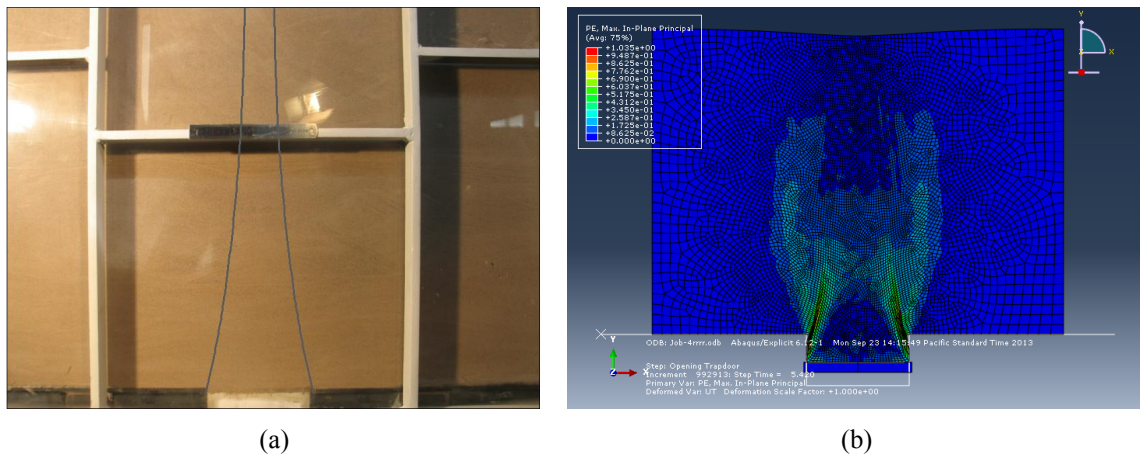(a)   (b)

Fig. 10 Comparing the experimental formation of arching and plastic contours for 20 cm trapdoor diameter ($D_r = 14\%$)

6. Results

The test results with 10, 20 and 30 cm width trapdoors for loose sand ($D_r = 14\%$) are depictedin Figs. 9-11, as examples. For comparing, at the right side of each picture (*b*) the contours of total plastic strain obtained from numerical study are presented. Regarding to the pictures the progress of the total plastic stain is same as shown in the experiments. In Figs 12-14, graphs of the σ/σ_0 (the ratio of normal stress applied on the trapdoor during any stage of yielding to the same stress at the initial state of trapdoor with no displacement) against trapdoor downward displacement (ΔH) both in experimental and numerical investigations are illustrated. The ratio σ/σ_0 defines stress reduction level due to arching effect, indeed.

7. Discussion

Referring to Figs. 12-14, it is observed that at the early stages of the trapdoor yielding, stress applied on the trapdoor due to soil weight decreases sharply as the trapdoor yields. At this stage

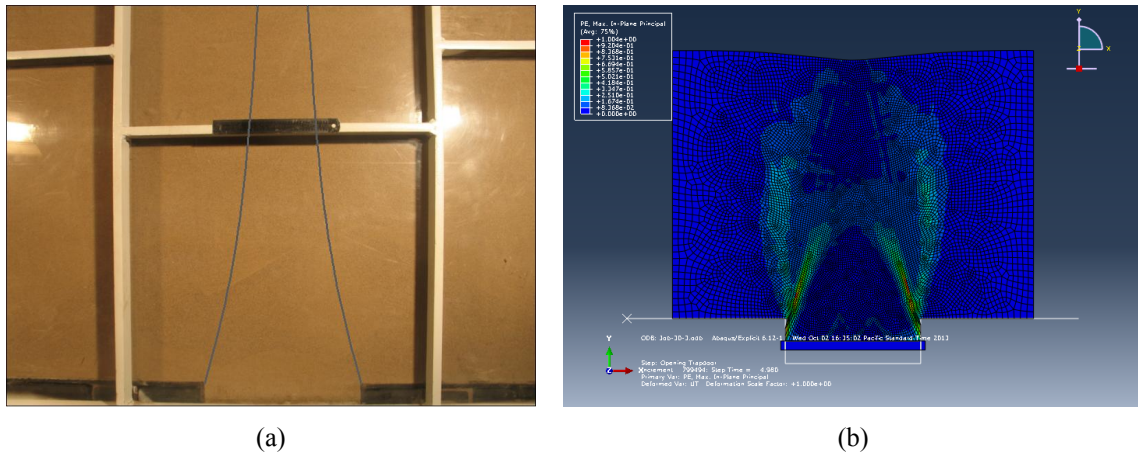(a)   (b)

Fig. 11 Comparing the experimental formation of arching and plastic contours for 30 cm trapdoor diameter ($D_r = 14\%$)
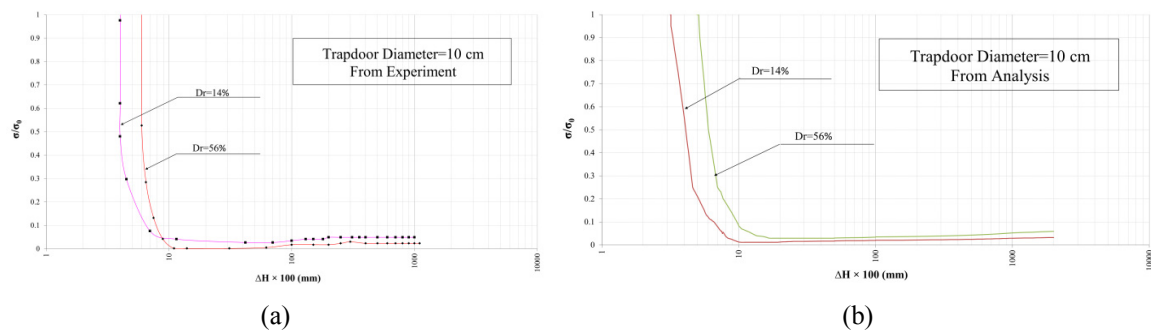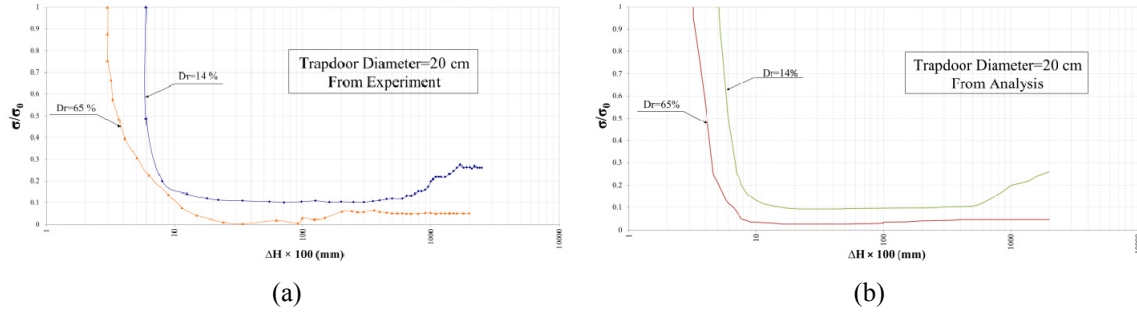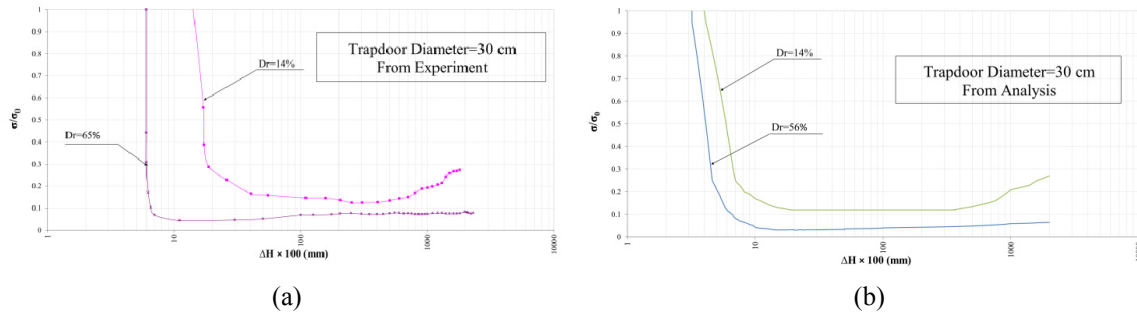

(a)   (b)

Fig. 12 Stress ratio-yield plots for 10 cm trapdoor diameter ($D_r = 14\%$ and 56%)

(a)   (b)

Fig. 13 Stress ratio-yield plots for 20 cm trapdoor diameter (D_r = 14.5% and 65%)

(a)   (b)

Fig. 14 Stress ratio-yield plots for 30 cm trapdoor diameter (D_r = 14% and 65%)

the whole mass of sand behaves mostly elastic. As the trapdoor yield proceeds, the stress ratio decreases and tends toward a minimum value, keeps on a constant level and then increases again until it tends toward an ultimate level. While a stable arch forms, the ultimate level tends to a constant value. But when an unstable arch mechanism occurs and the soil mass collapses progressively, the ultimate ratio displays increasing behavior. This behavior is true for all trapdoors. However, as the diameter of the trapdoor increases and/or the relative density of sand decreases, the minimum and ultimate stress ratios both increase. This behavior may be interpreted as follows. As the trapdoor yield starts the overlying soil weight, exerted by the trapdoor, is transmitted gradually onto the container base, surrounding the trapdoor. For this reason at initial stage of the trapdoor yielding, in which the sand mass behaves mostly elastic, a small yield is followed by a sharp decrease in the stress carried by the trapdoor. As the trapdoor yield proceeds, random plastic points in the sand mass deform. At this stage stress adjustment due to trapdoor yielding is not immediate and occurs with some time lag. This is attributed to the flow phenomenon that occurs due to the plastic behavior of the yielding sand mass. Then continuing the downward displacement and the stress ratio approaching a minimum value, failure occurs. At failure state, depending on the trapdoor diameter, relative density, and the dilation angle of the sand, the failing sand mass dilates which imposes further stress on the trapdoor and continues until the failure surface has developed and the yielded mass of sand is separated from the whole mass. Following this stage there is no longer any stress or mass exchange between two parts. Accordingly, the load cell displays a constant value. But when the formation and extension of the

plastic points are towards the soil surface, stress applying on the trapdoor increases and progressive failure is observed in the soil mass.

So that the kinematics involved during trapdoor opening break down into four distinct phases. These four phases have to be compared to the variation of the stress (σ) applied on the trapdoor with its displacement (ΔH). The failure boundaries of this area start at each edge of the trapdoor in vertical direction and then converge to axis of symmetry of the trapdoor, of course the inclination of this convergence is different depending on the sand's relative density and trapdoor diameter resulting in stable or unstable arch. In the initial state corresponds to the lowest stress applied on the trapdoor, the soil have elastic behavior. To this first state succeeds a flow phase so that the large strains occur in soil mass without considerable change in stress level. During this phase the plastic and failure boundaries extend to join together in the axis of symmetry of the trapdoor to produce a stable arch or extend to the top of the soil mass for unstable arch. In this phase, the extension of the plastic strain causes softening in the plastic zone of the soil mass while the inner part of the soil remains elastic and due to the increase in stress level in the adjacent parts with lower elastic and plastic strains, hardening phenomenon emerges. In the end of second phase, a transitional state is started. During this transition, total failure and separation in the two parts of the soil occurs. But in the stable arch this state leads to a constant trend of a stress level that indicates the fixed soil mass separated from the dome. But in the unstable arch increment in stress level continue because of the progressive failure in soil mass.

8. Conclusions

- Relative density of the soil and the trapdoor diameter, both are dominant factors affecting formation of a stable arch. As the trapdoor yields, following a small initial mostly elastic strain, the soil mass deforms plastically with larger strain rates and pressure applied onto the trapdoor decreases to a minimum value. Then, as the trapdoor yield continues, depending on the dilation angle and relative density of sand, stress level on the trapdoor increases gently and finally tends towards a constant value. At this stage the yielding sand mass separates from the whole mass.
- Referring to the experimental and numerical investigations, there are 4 phases in arching mechanism.
- The first phase occurs immediately after a small downward displacement of the trapdoor that leads to a minimum pressure applied to the trapdoor. During this stage soil mass behaves elastically.
- The second phase starts after the pressure on the trapdoor reaches a minimum value. This phase continues in a large period of plastic strains. In this state plastic strain and failure start at each edge of the trapdoor in vertical direction and then converge to axis of symmetry of the trapdoor, of course the inclination of this extension depends on the   relative density of sand and trapdoor diameter resulting in stable or unstable arch.   In second stage, flow phenomenon occurs in soil mass so that considering large strains in soil mass there is no considerable change in stress level.
- The third phase starts with an increment in stress applied on the trapdoor. The separation and establishment of a stable arch occurs at this stage. In the unstable arch manner, increment continues and the stress curve does not change its behavior to transfer to the fourth state.

- The fourth phase happens in stable arch manner so that stress ratio leads to a constant value. This indicates that the separation of stable arch is completed and trapdoor bears the whole weight of the separated arch mass.
- In Modeling the arching effect, the stress hardening in elastic strains and plastic strain hardening - softening behavior with Modified Mohr-Coulomb failure criteria can be used to model the realistic behavior of the sand especially flow phenomenon.

References

ABAQUS, Inc. (2012), ABAQUS V.6.12.1 user's manual.

Anastasopoulos, G., Gazetas, G., Bransby, M., Davies, M. and El Nahas, A. (2007), "Fault rupture propagation through sand: Finite-element analysis and validation through centrifuge experiments", *J. Geotech. Geoenviron. Eng.*, **133**(8), 943-958.

Ardakani, A., Bayat, M. and Javanmard, M. (2014), "Numerical modeling of soil nail walls considering Mohr Coulomb, hardening soil and hardening soil with small-strain stiffness effect models", *Geomech. Eng., Int. J.*, **6**(4), 391-401.

Atkinson, J.H. and Potts, D.M. (1977), "Stability of a shallow circular tunnel in cohesionless soil", *Geotechnique*, **27**(2), 203-215.

Bray, J.D., Seed, R.B., Cluff, L.S. and Seed, H.B. (1994), "Earthquake fault rupture propagation through soil." *J. Geotech. Engrg.*, **120**(3), 543-561.

Chen, R.P., Tang, L.J., Ling, D.S. and Chen, Y.M. (2011), "Face stability analysis of shallow shield tunnels in dry sandy ground using the discrete element method", *Comput. Geotech.*, **38** (2), 187-195.

Cole, D.A. Jr. and Lade, P.V. (1984), "Influence zones in alluvium over dip-slip faults", *J. Geotech. Eng.*, **110**(5), 599-615.

Dalvi, R.S. and Pise, R.J. (2012), "Analysis of arching in soil-passive state", *Indian Geotech. J.*, **42**(2), 106-112.

Dang, H.K. and Meguid, M.A. (2011), "An efficient finite-discrete element method for quasi-static nonlinear soil-structure interaction problems", *Int. J. Numer. Anal. Method. Geomech.*, **37**(2), 130-149. URL: http://onlinelibrary.wiley.com/doi/10.1002/nag.1089/pdf

Gudehus, G. and Nübel, K. (2004), "Evolution of shear bands in sand", *Geotechnique*, **54**(3), 187-201.

Hosseinian, S. and Cheraghi Seifabad, M. (2013), "Optimization the distance between piles in supporting structure using soil arching effect", *J. Civil Eng. Urban.*, **3**(6), 386-391.

Jewell, R.A. (1989), "Direct shear tests on sand", *Geotechnique*, **39**(2), 309-322.

Jewell, R.A. and Roth, C.P. (1987), "Direct shear tests on reinforced sand", *Geotechnique*, **37**(1), 53-68.

Kim, K.Y., Lee, D.S., Cho, J., Jeong, S.S. and Lee, S. (2013), "The effect of arching pressure on a vertical circular shaft", *Tunn. Undergr. Space Technol.*, **37**, 10-21.

Mahin Roosta, R. and Alizade, A, (2012), "Simulation of collapse settlement in rockfill material due to saturation", *Int. J. Civil Eng.*, **10**(2), 102-108.

Muir Wood, D. (2002), "Some observations of volumetric instabilities in soils", *Int. J. Solids Struct.*, **39**(13-14), 3429-3449.

Muir Wood, D. and Stone, K.J.L. (1994), "Some observations of zones of localization in model tests on dry sand", In: *Localization and Bifurcation Theory for Soils and Rocks*, (R. Chambon, J. Desrues, and I. Vardoulakis, Eds.), Balkema, Rotterdam, Netherlands, pp. 155-164.

Otani, J. and Chevalier, B. (2010), "3-D arching effect in the trap-door problem: A comparison between X-ray CT scanning and DEM analysis", *GeoFlorida*, 570-579.

Pardo, G.S. and Sáez, E. (2014), "Experimental and numerical study of arching soil effect in coarse sand", *Comput. Geotech.*, **57**, 75-84.

Pietruszezak, S.T. and Mroz, Z. (1981), "Finite-element analysis of deformation of strain softening materials", *Int. J. Numer. Methods Eng.*, **17**(3), 327-334.

Rowe, P.W. (1963), "Stress-dilatancy, earth pressure and slopes", *J. Soil Mech. Found. Div.*, *ASCE*, **89**(5), 37-61.

Sardrekarimi, J. and Abbasnejad, A.R. (2008), "An experimental investigation into the arching effect in fine sand", *Int. J. Eng.*, **21**(4), 345-360.

Sadrekarimi, J. and Abbasnejad, A.R. (2010), "Arching effect in fine sand due to base yielding", *Can. Geotech. J.*, **47**(3), 366-374.

Sardrekarimi, J., Moradi, G. and Abbasnejad, A.R. (2010), "Studying and comparing the experimental and numerical investigation on to the arching effect in fine sand using PlAXIS code and Mohr-coulomb criteria", *Proceeding of the 4th International Conference on Geotechnical Engineering*, Tehran, Iran.

Shibuya, S., Mitachi, T. and Tamate, S. (1997), "Interpretation of direct shear box testing of sands as quasisimple shear", *Geotechnique*, **47**(4), 769-790.

Soreide, O.K., Nordal, S. and Bonnier, P.G. (2002), "An implicit friction hardening model for soil materials", (Mestat Ed.), *Numer. Method. Geotech. Eng.*, *NUMGE*, 155-161.

Terzaghi, K. (1943), *Theoritical Soil Mechanics*, JohnWiley and Sons Inc., New York, NY, USA.

Vardoulakis, I. and Graf, B. (1985), "Calibration of constitutive models for granular materials using data from biaxial experiments", *Geotechnique*, **35**(3), 299-317.

Vardoulakis, I., Graf, B. and Gudehus, G. (1981), "Trapdoor problem with dry sand: A statical approach based upon model test kinematics", *Int. J. Numer. Anal. Method. Geomech.*, **5**(1), 57-78.

Vermeer, P.A. and de Borst, R. (1984), "Non-associated plasticity for soils, concrete and rock", *Heron 29*, **3**.

Wroth, C.P. (1979), "Correlations of some engineering properties of soil", *Acta Informatica*: *Proceedings of International Conference on the Behaviour of Off-Shore Structures*, London, England, August, pp. 121-132.

Wroth, C.P. and Houlsby, G.T. (1985), "Soil mechanics – Property characterization and analysis procedures", *Proceedings of the 11th International Conference on Soil Mechanics and Foundation Engineering*, San Francisco, CA, USA, August, Volume 1, pp. 1-55.

CC